

## **ELECTROMAGNETIC DESIGN AND ANALYSIS OF DOUBLE-ROTOR FLUX-MODULATED PERMANENT-MAGNET MACHINES**

**C. Liu<sup>\*</sup> and K. T. Chau**

Department of Electrical and Electronic Engineering, The University of Hong Kong, Pokfulam Road, Hong Kong, China

**Abstract**—Two double-rotor flux-modulated permanent-magnet (DR-FMPM) machines are proposed for direct-drive applications, including the DR coaxial magnetic-gearing (CMG) type and the DR PM vernier (PMV) type. The key of the DR-CMG type is to utilize two modulation rings for obtaining the desired magnetic-gearing effect, whereas the key of the DR-PMV type is to utilize the flux-modulation poles and fractional-slot concentrated-winding arrangement for achieving the magnetic-gearing effect. Thus, both proposed machines are able to directly connect their rotors with two different rotating loads. Their rotating speeds can also be independently controlled by two sets of armature windings. The proposed machines are designed and then analyzed by using the time-stepping finite element method. The corresponding results confirm the validity of the proposed machine design.

### **1. INTRODUCTION**

Electric machines serving as the core component for electromechanical energy conversion play a significant role in modern industry development [1, 2]. Differing from the fast development of traditional single-rotor machines, double-rotor (DR) machines have taken slow development. With ever increasing applications of two rotating loads, the development of DR machines is accelerated. For instance, the two rotors are separately connected to the left and right wheels of electric vehicles [3], hence performing electronic differential action [4]. Also, the two rotors are used to perform power split of the internal combustion engine [5], hence achieving optimal operation for hybrid electric vehicles [6]. Similarly, they are utilized to split the output

---

*Received 6 June 2012, Accepted 16 August 2012, Scheduled 4 September 2012*

\* Corresponding author: Chunhua Liu (chualiu@eee.hku.hk).

power of wind turbine, hence obtaining optimal efficiency for wind energy harvesting [7].

Recently, flux-modulated permanent-magnet (FMPM) machines attract much attention for direct-drive applications due to their unique feature of magnetic-gearing effect [8, 9]. Apart from incorporating the coaxial magnetic gear (CMG) to provide the magnetic-gearing effect [10–12], the FMPM machines can utilize the PM vernier (PMV) principle to produce the magnetic-gearing effect [13–15]. Differing from the traditional PM machines, the FMPM machines employ electromagnetic field modulation to realize torque transmission and speed control. The CMG machines possess the merit of straightforward combination of the magnetic gear and the PM machine, but suffer from the drawback of three air gaps. In contrast, the PMV machines take the merit of involving only one air-gap, but desire a dedicated structure.

The purpose of this paper is to propose and compare two novel types of FMPM machines, namely the DR-CMG type and the DR-PMV type. Differing from the previous FMPM machines, the proposed two machines adopt the DR structure and involve two effective air-gaps. Hence, they can achieve higher output torque, smaller torque ripple, lower cogging torque and better direct-drive performance than the previous FMPM machines. Specifically, the DR-CMG machine will utilize two modulation-rings (MRs) to perform the desired magnetic field modulation, whereas the DR-PMV machine will adopt flux-modulation poles (FMPs) and the fractional-slot concentrated-winding (FSCW) arrangement to accomplish the magnetic field modulation. In order to fairly compare their performances, both machines will be designed under the same constraints. In addition, the machine performances will be analyzed by using the time-stepping finite element method (TS-FEM).

## 2. MACHINE STRUCTURE

Figure 1 shows the structures of the proposed DR-FMPM machines. It can be seen that the DR-CMG type consists of two rotors, two MRs and one stator. The PMs are mounted on the inside surface and the outside surface of the outer rotor and the inner rotor, respectively. The stator is sandwiched between two MRs, which also accommodates two sets of armature windings. Each MR is located between the rotor and the stator, which functions to modulate the magnetic field distribution. The outer rotor generally runs at low speeds for direct driving. So, its low-speed PM rotating field is modulated by the outer MR to the high-speed outer armature winding field. Meanwhile, the inner rotor, inner MR, and inner armature winding have the same field modulation effect.

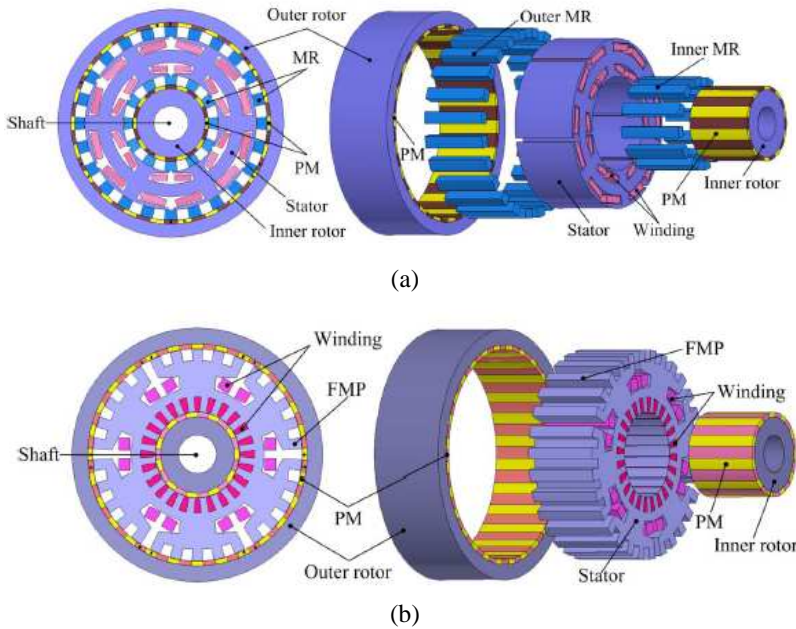


**Figure 1.** Proposed DR-FMPM machines. (a) DR-CMG type. (b) DR-PMV type.

The magnetic-gearing ratios of the outer rotor and inner rotor can be designed to be the same or different, depending on the types of direct-drive applications. Finally, the inner rotor speed and outer rotor speed can be independently controlled by their respective armature windings located in the stator.

On the other hand, it can be found that the DR-PMV type has two rotors and one dedicated stator. The PMs are also mounted on the inside surface and the outside surface of the outer rotor and the inner rotor, respectively. The stator incorporates dedicated FMPs and the FSCW arrangement. When the outer rotor operates at low speeds, the low-speed PM rotating field is modulated by the FMPs to the high-speed outer armature winding field. Meanwhile, the inner rotor generally runs at high speeds so that the PM rotating field directly interacts with the inner armature winding field. Thus, the two rotor speeds and hence the corresponding magnetic-gearing ratios are different. Of course, the inner rotor speed and outer rotor speed can be independently controlled by their respective armature windings located in the stator.

In order to fairly evaluate the proposed two machines, they obey

the following design rules:

- Both machines have the same outside diameter and axial length.
- Both machines adopt the same grade of iron and copper materials and the same type of PM material.
- The calculation environment and conditions of TS-FEM are the same for both machines.

### 3. OPERATION PRINCIPLE

Since both the DR-CMG machine and DR-PMV machine belong to the class of FMPM machines, their pole-pair arrangements are governed by:

$$\omega_{j,k} = \frac{j p_s}{|j p_s + k N_{\text{mod}}|} \omega_s, \quad p_{j,k} = |j p_s + k N_{\text{mod}}| \quad (1)$$

where  $j = 1, 3, 5, \dots$ ,  $k = 0, \pm 1, \pm 2, \dots$ ,  $\omega_s$  is the rotating field speed of the stator armature winding,  $p_s$  the pole-pair number of the stator armature winding, and  $N_{\text{mod}}$  the number of segments of the MR for the DR-CMG machine or the number of poles of the FMP for the DR-PMV machine. In order to transmit the torque from the armature field of the stator to the rotating field of the rotor, the rotor speed  $\omega_r$  and the number of PM pole-pairs in the rotor  $p_r$  should be equal to  $\omega_{j,k}$  and  $p_{j,k}$ , respectively. When  $j = 1$  and  $k = -1$ , the largest space harmonic component is attained for torque transmission. Thus, the corresponding airgap flux density space harmonics and the pole-pair number can be rewritten as:

$$\omega_r = \frac{p_s}{|p_s - N_{\text{mod}}|} \omega_s, \quad p_r = |p_s - N_{\text{mod}}| \quad (2)$$

In addition, the relationship between the  $N_{\text{mod}}$  and the  $p_s$  can be expressed as:

$$N_{\text{mod}} = m \times i_o \times p_s \quad (3)$$

where  $m$  is the number of phases and  $i_o$  (usually,  $i_o = 2, 3, 4, \dots$ ) the number of MR segments or FMPs per armature winding pole per phase.

For the DR-CMG machine, when the parameters of the outer MR and the outer armature winding are selected as  $m = 3$ ,  $p_s = 2$  and  $N_{\text{mod}} = 24$ , it yields  $p_r = 22$ . Hence, the magnetic-gearing ratio between the outer rotor speed and the outer armature field speed is  $G_r = 1/11$  which denotes that the outer rotor speed is only 1/11 of the outer armature rotating field speed in the stator. For instance, when the outer armature field speed is 2200 rpm, the outer rotor speed is scaled down to 200 rpm. Meanwhile, when the parameters of the inner

MR and the inner armature winding are selected as  $m = 3$ ,  $p_s = 2$  and  $N_{\text{mod}} = 12$ , it yields  $p_r = 10$ . Hence, the corresponding magnetic-gearing ratio is  $G_r = 1/5$ . Namely, when the speed of inner armature field is 2200 rpm, the inner rotor speed is scaled down to 440 rpm.

For the DR-PMV machine, when the parameters of the FMPs and the outer armature winding are selected as  $m = 3$ ,  $p_s = 2$  and  $N_{\text{mod}} = 30$ , it deduces  $p_r = 28$ . Hence, the corresponding magnetic-gearing ratio is  $G_r = 1/14$  indicating that the outer rotor speed is 1/14 of the outer armature field speed. Meanwhile, the inner rotor and the inner armature winding adopt another relationship of pole-pair arrangement as given by:

$$2p_{r\_FSCW} = N_{s\_FSCW} - 2p_{s\_FSCW} \tag{4}$$

where  $p_{r\_FSCW}$  is the number of PM polepairs in the inner rotor,  $p_{s\_FSCW}$  the number of polepairs of the inner armature winding in the stator, and  $N_{s\_FSCW}$  the number of the inner armature winding slots. Hence, when  $p_{s\_FSCW} = 1$  and  $N_{s\_FSCW} = 24$  are selected, it yields  $p_{r\_FSCW} = 11$ .

Figure 2 shows the armature winding connection of the proposed DR-FMPM machines. Both of the two armature windings of the DR-CMG type and the outer armature winding of the DR-PMV type adopt the 6-slot arrangement in which the winding connections are arranged as  $+A, -A, +B, -B, +C, -C, +A, -A, +B, -B, +C,$  and  $-C$ . In

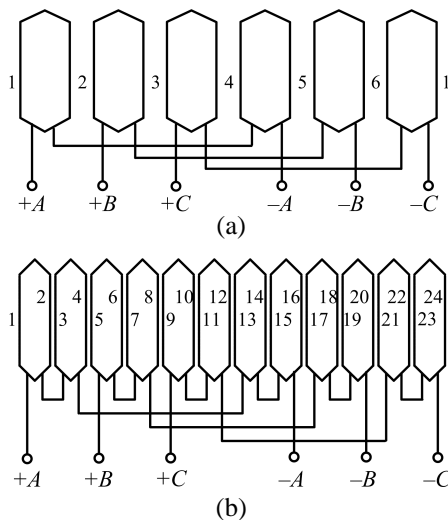


**Figure 2.** Winding connection diagram. (a) 6-slot arrangement. (b) 24-slot arrangement.

contrast, the inner armature winding of the DR-PMV type adopts the 24-slot arrangement in which the connections are arranged as  $+A, -A, +A, -A, +C, -C, +C, -C, +B, -B, +B, -B, -A, +A, -A, +A, -C, +C, -C, +C, -B, +B, -B, +B$ . It can be seen that the DR-CMG machine has larger slots in the stator to accommodate more copper conductors than the traditional PM machine, hence improving the machine power density. While the outer armature winding of the DR-PMV machine has the same connection as that of the DR-CMG machine, the corresponding inner armature winding occupies a larger number of slots, thus suffering from smaller slots. Nevertheless, its FSCW arrangement helps reduce the torque ripple [16].

The key design data of the proposed two DR-FMPM machines are summarized in Table 1.

**Table 1.** Key design data of DR-FMPM machines.

Item	DR-CMG type	DR-PMV type
Outer rotor outside diameter	264.0 mm	264.0 mm
Outer rotor inside diameter	225.2 mm	221.2 mm
Inner rotor outside diameter	88.0 mm	88.0 mm
Inner rotor inside diameter	40.0 mm	40.0 mm
Stator outside diameter	200.0 mm	220.0 mm
Stator inside diameter	111.2 mm	89.2 mm
MR outside diameter	224.0 mm	-
MR inside diameter	201.2 mm	-
MR pitch angle	22.0 degree	-
FMP height	-	12.0 mm
FMP pitch angle	-	6.0 degree
Air-gap length	0.6 mm	0.6 mm
Axial length	80.0 mm	80.0 mm
Number of outer rotor PM pole-pairs	22	28
Number of inner rotor PM pole-pairs	10	11
Number of outer MR segments	24	-
Number of inner MR segments	12	-
Number of FMPs	-	30
Number of outer armature winding slots	6	6
Number of inner armature winding slots	6	24
Outer armature winding per slot per phase	80 turns	80 turns
Inner armature winding per slot per phase	80 turns	40 turns
PM material (remanence)	NdFeB (1.2 T)	NdFeB (1.2 T)

#### 4. ELECTROMAGNETIC FIELD ANALYSIS

Electromagnetic field analysis has been widely developed for electric machines. Basically, it can be categorized as analytical field calculation [17] and numerical field calculation [18]. The FEM is the one of the most popular numerical field calculation tools. In this paper, the TS-FEM is developed for analyzing the proposed DR-FMPM machines. In general, the calculation model for the motoring mode of electric machines consists of three types of equations: the electromagnetic field equation of the machine, the circuit equation of the armature circuit, and the motion equation of the mechanical drive system. It should be noted that the calculation model involves only the first two types of equations for the generation mode.

Firstly, the electromagnetic field equations of the proposed machines are governed by:

$$\nabla \times (\nu \nabla \times A) = J \quad (5)$$

where  $\nu$  is the reluctivity,  $J$  the current density, and  $A$  the magnetic vector potential. Since the end effect of the proposed machines is not significant, the two-dimensional analysis is preferred. So, both  $J$  and  $A$  have only the  $z$ -axis components. The corresponding electromagnetic field equation can be written as:

$$\Omega : \frac{\partial}{\partial x} \left( v \frac{\partial A}{\partial x} \right) + \frac{\partial}{\partial y} \left( v \frac{\partial A}{\partial y} \right) = -J - v \left( \frac{\partial B_{ry}}{\partial x} - \frac{\partial B_{rx}}{\partial y} \right) + \sigma \frac{\partial A}{\partial t} \quad (6)$$

$$S_1 : A = A_{z0} = 0 \quad (7)$$

where  $\Omega$  is the field solution region,  $\sigma$  the electrical conductivity,  $B_{rx}$  the  $x$ -axis component of the PM remanent flux density, and  $B_{ry}$  the  $y$ -axis component of the PM remanent flux density. Along the outside periphery of the machines, the magnetic vector potential is assumed to be zero.

Secondly, the circuit equation during motoring is given by

$$u = Ri + L_e \frac{di}{dt} + e \quad (8)$$

$$e = \frac{l}{S} \iint_{\Omega_e} \frac{\partial A}{\partial t} d\Omega \quad (9)$$

where  $u$  is the applied voltage,  $R$  the resistance per phase winding,  $L_e$  the inductance of the end winding,  $e$  the electromotive force (EMF) per phase,  $i$  the phase current,  $l$  the axial length of iron core,  $S$  the conductor area of each turn of phase winding, and  $\Omega_e$  the total cross-sectional area of conductors of each phase winding. On the other hand,

the circuit equation during generation is governed by:

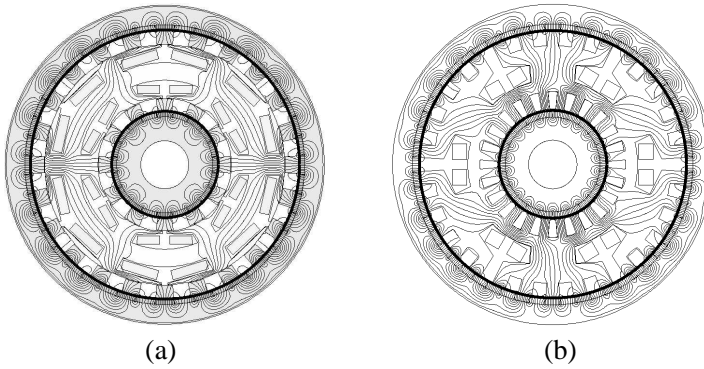
$$u = e - Ri - L_e \frac{di}{dt} \quad (10)$$

where  $u$  stands for the generated voltage. So, it can be seen that the circuit equation is similar with that for motoring, except the direction of  $i$ .

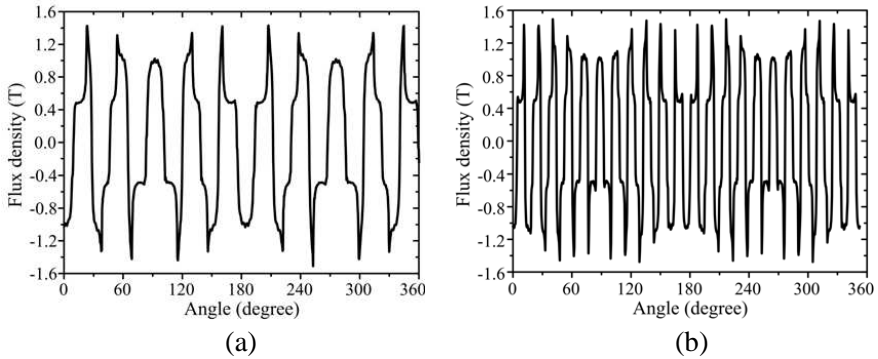
The motion equation of the machine is given by:

$$J_m \frac{d\omega}{dt} = T_e - T_L - \lambda\omega \quad (11)$$

where  $J_m$  is the moment of inertia,  $\omega$  the mechanical speed,  $T_L$  the load torque, and  $\lambda$  the damping coefficient.



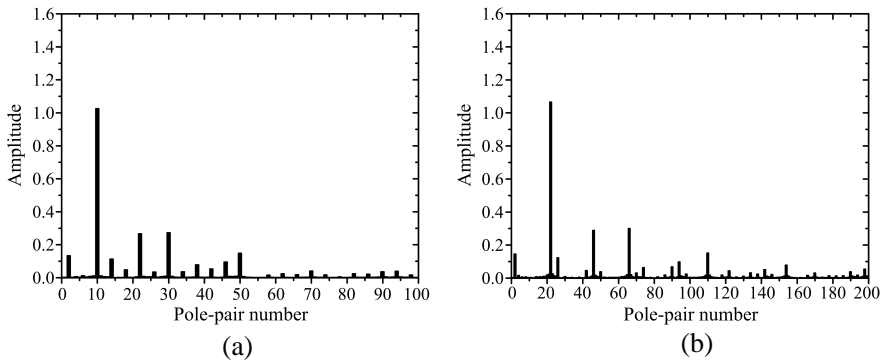
**Figure 3.** No-load magnetic field distributions. (a) DR-CMG type. (b) DR-PMV type.



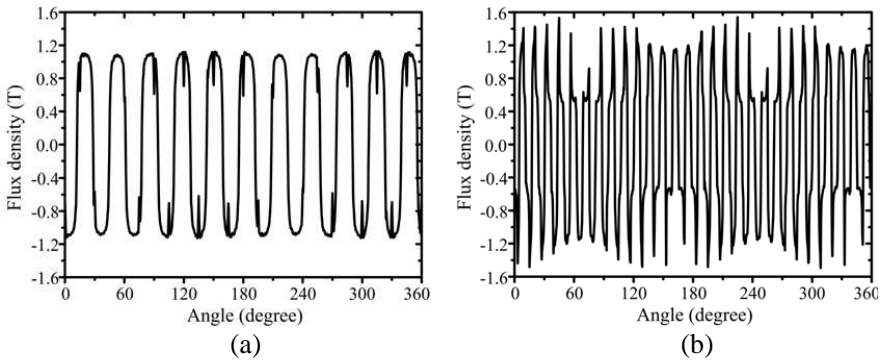
**Figure 4.** Air-gap flux density waveforms of DR-CMG machine. (a) Inner air-gap. (b) Outer air-gap.

Therefore, after discretization, the three types of equations can be solved at each time step. Consequently, both steady-state and transient performances of the proposed machines can be calculated.

Figure 3 shows the magnetic field distributions of both machines under no-load condition. It can be observed that with the use of MRs, the magnetic flux of the sandwiched stator of the DR-CMG machine can go through the PM poles properly, hence illustrating the desired flux modulation effect. On the other hand, it can be seen that with the use of FMPs, the same flux modulation effect occurs between the outer stator and the outer rotor of the DR-PMV machine. Meanwhile, the magnetic flux of the inner stator can directly go through the inner rotor.



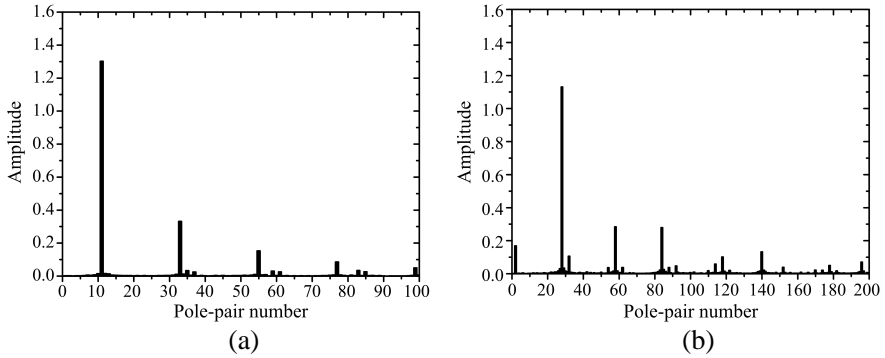
**Figure 5.** Air-gap flux density harmonic spectra of DR-CMG machine. (a) Inner air-gap. (b) Outer air-gap.



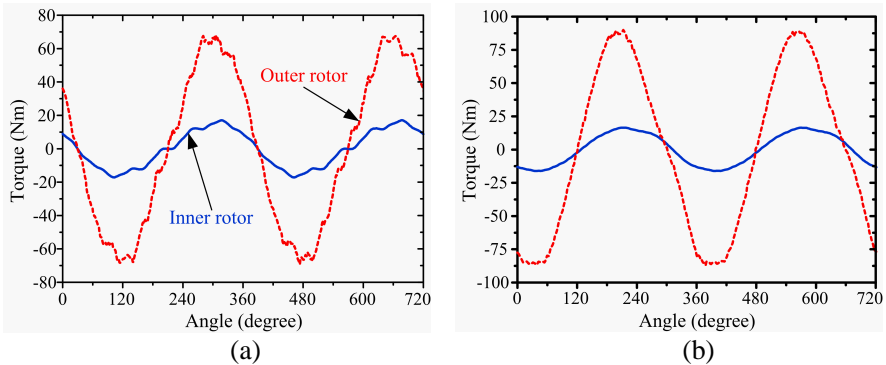
**Figure 6.** Air-gap flux density waveforms of DR-PMV machine. (a) Inner air-gap. (b) Outer air-gap.

Figure 4 shows the radial air-gap flux density waveforms of the DR-CMG machine under no-load condition. By applying the fast Fourier transform (FFT) to these waveforms, the corresponding harmonic spectra are deduced as shown in Figure 5. It can be observed that they mainly exhibit 10 polepairs in the inner air-gap and 22 polepairs in the outer air-gap, both correspond to 2 polepairs of the armature winding fields in the stator. Hence, it validates the DR-CMG machine design described by (2) and (3). Similarly, Figure 6 and Figure 7 show the radial air-gap flux density waveforms and the corresponding harmonic spectra of the DR-PMV machine under no-load condition, respectively. It can be seen that they mainly exhibit 11 polepairs in the inner air-gap and 28 polepairs in the outer air-gap, hence validating the DR-PMV machine design.

In order to evaluate the torque transmission capability of the outer



**Figure 7.** Air-gap flux density harmonic spectra of DR-PMV machine. (a) Inner air-gap. (b) Outer air-gap.



**Figure 8.** Torque-angle curves. (a) DR-CMV machine. (b) DR-PMV machine.

rotor and the inner rotor, the torque-angle curves of both DR-FMPM machines are calculated as depicted in Figure 8. These curves are deduced by rotating the rotors step by step while keeping the phase currents at  $8A$ ,  $-4A$  and  $-4A$  for both the inner and outer armature windings. It can be observed that the DR-CMG machine can produce the torque up to  $17.6Nm$  and  $68.7Nm$  at its inner rotor and outer rotor, respectively. Meanwhile, the DR-PMV machine can produce the torque up to  $16.5Nm$  and  $90.1Nm$  at its inner rotor and outer rotor, respectively. Hence, the DR-PMV machine can offer higher outer rotor torque than the DR-CMG machine, whereas their inner rotor torques are quite similar. It is due to the fact that the DR-PMV machine possesses a larger magnetic-gearing ratio at the outer rotor.

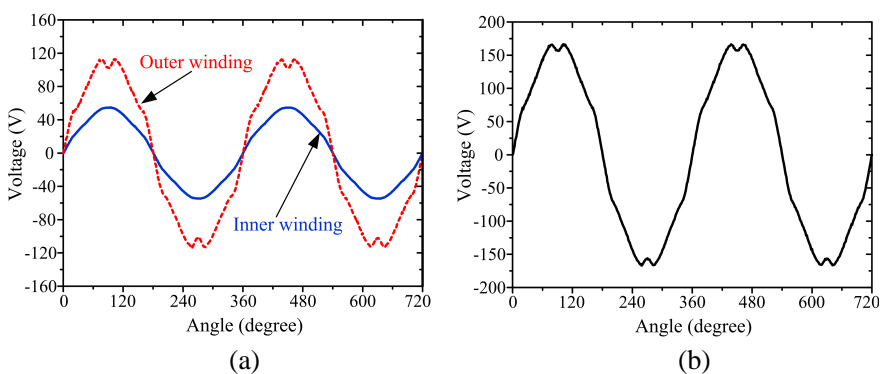


**Figure 9.** No-load EMF waveforms of DR-CMG machine at outer rotor speed of 200 rpm. (a) Separate. (b) Resultant.

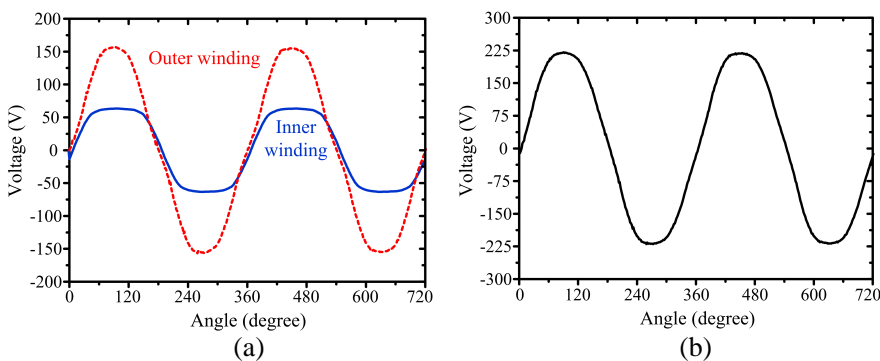


**Figure 10.** No-load EMF waveforms of DR-CMG machine at outer rotor speed of 200 rpm. (a) Separate. (b) Resultant.

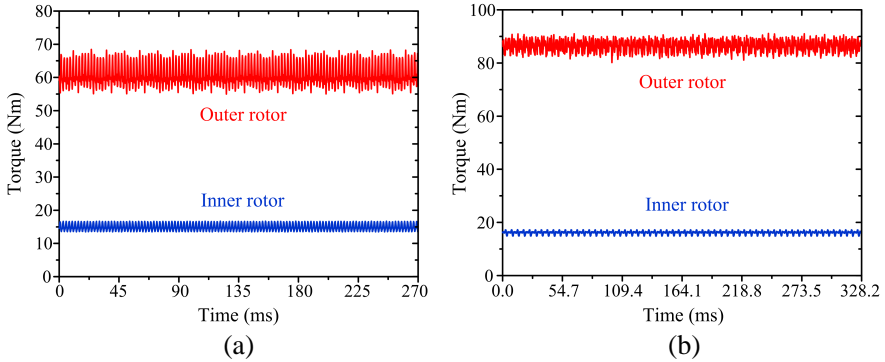


**Figure 11.** Output torque waveforms. (a) DR-CMV machine. (b) DR-PMV machine.

## 5. PERFORMANCE COMPARISON

Firstly, the generating performances of the proposed two DR-FMPM machines are assessed. Figure 9 and Figure 10 show the no-load EMF waveforms of both proposed machines under the same outer rotor speed of 200 rpm. It can be observed that the DR-CMG machine can generate up to 54.8 V at the inner armature winding and 113.8 V at the outer armature winding. Meanwhile, the DR-PMV machine can generate up to 63.4 V at the inner armature winding and 157.4 V at the outer armature winding. Consequently, the DR-CMG machine can achieve the resultant amplitude of 167.3 V, whereas the DR-PMV one can achieve the resultant amplitude of 220.6 V. It confirms that the DR-PMV machine can offer much higher no-load EMF.

Secondly, the motoring performances of the two machines are assessed. Figure 11 shows their output torque waveforms under the rated current of 8 A. It can be observed that the DR-CMG machine can produce the average torque of 16.6 Nm and 60.8 Nm at the inner rotor and outer rotor, respectively. In contrast, the DR-PMV machine can offer the average torque of 16.0 Nm and 86.4 Nm at the inner rotor and outer rotor, respectively. It confirms that the DR-PMV machine can offer much higher output torque at the outer rotor than the DR-CMG type, while their output torques at the inner rotor are similar. Moreover, the cogging torques of both DR-FMPM machines are calculated as depicted in Figure 12. It indicates that both machines exhibit the merit of small cogging torques, which is actually due to the inherit merit of multi-pole structures. Furthermore, the cogging torques of the DR-PMV type are further smaller than those of the

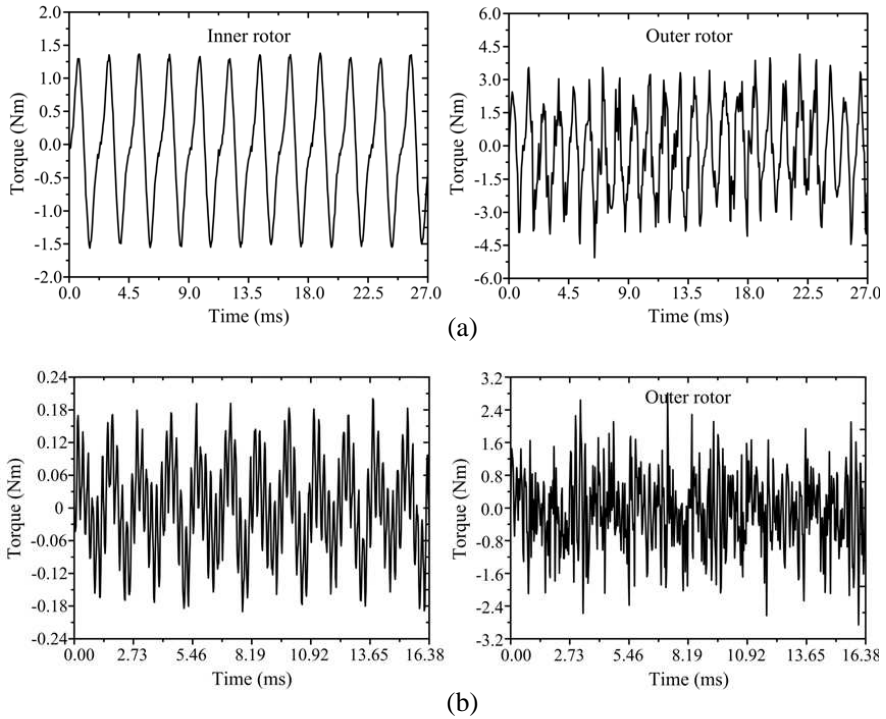


**Figure 12.** Cogging torque waveforms. (a) DR-CMV machine. (b) DR-PMV machine.

DR-CMG type, since the DR-PMV one adopts more PM pole-pairs.

Finally, their performance comparison is summarized in Table 2. It indicates that the proposed machines can offer very high torque densities, which are up to  $13884 \text{ Nm/m}^3$  at the outer rotor of the DR-CMG type and  $19730 \text{ Nm/m}^3$  at the outer rotor of the DR-PMV type. Also, their torque ripples are relatively small, which are only up to 22.0% at the outer rotor of the DR-CMG type and 14.9% at the inner rotor of the DR-PMV type. In addition, their cogging torques are very small, which are only up to 8.3% at the inner rotor of the DR-CMG machine and 3.3% at the outer rotor of the DR-PMV machine. Thus, it confirms that the use of FMPs and the FSCW arrangement for the DR-PMV machine can suppress the torque ripple and cogging torque better than the use of MRs for the DR-CMG machine.

**Table 2.** Performance comparison of DR-FMPM machines.

Item	DR-CMG type	DR-PMV type
Rated power	1900 W	2400 W
Rated current of inner and outer windings	8 A	8 A
Rated speed of inner rotor	440 rpm	500 rpm
Rated speed of outer rotor	200 rpm	200 rpm
Rated torque of inner rotor	16.6 Nm	16.0 Nm
Rated torque of outer rotor	60.8 Nm	86.4 Nm
Maximum torque of inner rotor	17.6 Nm	16.5 Nm
Maximum torque of outer rotor	68.7 Nm	90.1 Nm
Magnetic-gearing ratio of inner rotor	1/5	-
Magnetic-gearing ratio of outer rotor	1/11	1/14
Machine efficiency	87.2%	88.3%
Torque density of inner rotor	3790 Nm/m <sup>3</sup>	3654 Nm/m <sup>3</sup>
Torque density of outer rotor	13884 Nm/m <sup>3</sup>	19730 Nm/m <sup>3</sup>
Torque ripple at rated load of inner rotor	19.6%	14.9%
Torque ripple at rated load of outer rotor	22.0%	12.7%
Cogging torque / rated torque of inner rotor	8.3%	1.3%
Cogging torque / rated torque of outer rotor	7.2%	3.3%

## 6. CONCLUSION

This paper has proposed two DR-FMPM machines, namely the DR-CMG type and the DR-PMV type, for direct-drive applications. The DR-CMG type employs double MRs to produce the desired magnetic-gearing effect, whereas the DR-PMV type utilizes the FMPs and FSCW arrangement to obtain the magnetic-gearing effect. Both machines can produce high output torque densities with small torque ripples and cogging torques. Between them, the DR-PMV machine offers better performances than the DR-CMG type. These DR-FMPM machines have high potentiality for electric vehicle propulsion and renewable energy harvesting.

## NOMENCLATURE

$A$ : Magnetic vector potential.

$B_{rx}$ : The  $x$ -axis component of the PM remanent flux density.

$B_{ry}$ : The  $y$ -axis component of the PM remanent flux density.

$e$ : The electromotive force (EMF) per phase.

$G_r$ : Magnetic-gearing ratio.

- $i$ : Phase current.
- $i_o$ : Number of MR segments or FMPs per armature winding pole per phase.
- $J$ : Current density.
- $J_m$ : The moment of inertia.
- $l$ : The axial length of machine iron core.
- $L_e$ : Inductance of the end winding.
- $m$ : Number of machine phases.
- $N_{\text{mod}}$ : Number of segments of the MR for the DR-CMG machine or number of poles of the FMP for the DR-PMV machine.
- $N_{s\_FSCW}$ : Number of the inner armature winding slots for the DR-PMV machine.
- $p_{j,k}$ : Pole-pair number of the space harmonic component.
- $p_r$ : Number of PM pole-pairs in the rotor.
- $p_s$ : Pole-pair number of the stator armature winding.
- $p_{r\_FSCW}$ : Number of PM polepairs in the inner rotor for the DR-PMV machine.
- $p_{s\_FSCW}$ : Number of polepairs of the inner armature winding in the stator for the DR-PMV machine.
- $R$ : Resistance per phase winding.
- $S$ : The conductor area of each turn of phase winding.
- $T_L$ : The load torque.
- $u$ : The applied or generated voltage.
- $\omega$ : The mechanical speed.
- $\omega_{j,k}$ : Rotating speed of the space harmonic component.
- $\omega_r$ : Rotor speed.
- $\omega_s$ : Rotating field speed of the stator armature winding.
- $\nu$ : Reluctivity.
- $\Omega$ : Field solution region.
- $\Omega_e$ : The total cross-sectional area of conductors of each phase winding.
- $\sigma$ : Electrical conductivity.
- $\lambda$ : The damping coefficient.

## ACKNOWLEDGMENT

This work was supported by a research grant (Project No. HKU710612E) from the Research Grants Council in Hong Kong Special Administrative Region, China.

## REFERENCES

1. Chau, K. T., C. C. Chau, and C. Liu, "Overview of permanent magnet brushless drives for electric and hybrid electric vehicles," *IEEE Transactions on Industrial Electronics*, Vol. 55, No. 6, 2246–2257. Jun. 2008.
2. Zhu, Z. Q. and D. Howe, "Electrical machines and drives for electric, hybrid and fuel cell vehicles," *Proceedings of IEEE*, Vol. 95, No. 4, 746–765, Apr. 2007.
3. Kawamura, A., N. Hoshi, T. W. Kim, T. Yokoyama, and T. Kume, "Analysis of anti-directional-twin-rotary motor drive characteristics for electric vehicles," *IEEE Transactions on Industrial Electronics*, Vol. 44, No. 1, 64–70, Feb. 1997.
4. Chan, C. C. and K. T. Chau, *Modern Electric Vehicle Technology*, Oxford University Press, Nov. 2001.
5. Hoeijmakers, M. J. and J. A. Ferreira, "The electric variable transmission," *IEEE Transactions on Industry Applications*, Vol. 42, No. 4, 1092–1100, Jul.–Aug. 2006.
6. Chau, K. T. and C. C. Chan, "Emerging energy-efficient technologies for hybrid electric vehicles," *Proceedings of IEEE*, Vol. 95, No. 4, 821–835, Apr. 2007.
7. Sun, X., M. Cheng, W. Hua, and L. Xu, "Optimal design of double-layer permanent magnet dual mechanical port machine for wind power application," *IEEE Transactions on Magnetics*, Vol. 45, No. 10, 4613–4616, Oct. 2009.
8. Atallah, K. and D. Howe, "A novel high-performance magnetic gear," *IEEE Transactions on Magnetics*, Vol. 37, No. 4, 2844–2846, Jul. 2001,
9. Jian, L. and K.-T. Chau, "Analytical calculation of magnetic field distribution in coaxial magnetic gears," *Progress In Electromagnetics Research*, Vol. 92, 1–16, 2009.
10. Chau, K. T., D. Zhang, J. Z. Zhang, C. Liu, and Y. J. Zhang, "Design of a magnetic-geared outer-rotor permanent-magnet brushless motor for electric vehicles," *IEEE Transactions on Magnetics*, Vol. 43, No. 6, 2504–2506, Jun. 2007.
11. Jian, L., K. T. Chau, and J. Z. Jiang, "A magnetic-geared outer-rotor permanent-magnet brushless machine for wind power generation," *IEEE Transactions on Industry Applications*, Vol. 45, No. 3, 954–962, May/June. 2009.
12. Jian, L. and K.-T. Chau, "Design and analysis of a magnetic-geared electronic-continuously variable transmission system using finite element method," *Progress In Electromagnetics Research*,

Vol. 107, 47–61, 2010.

13. Toba, A. and T. A. Lipo, “Generic torque-maximizing design methodology of surface permanent-magnet vernier machine,” *IEEE Transactions on Industry Applications*, Vol. 36, No. 6, 1539–1546, Nov./Dec. 2000.
14. Li, J., K. T. Chau, J. Z. Jiang, C. Liu, and W. Li, “A new efficient permanent-magnet vernier machine for wind power generation,” *IEEE Transactions on Magnetics*, Vol. 46, No. 6, 1475–1478, Jun. 2010.
15. Liu, C., J. Zhong, and K. T. Chau, “A novel flux-controllable vernier permanent-magnet machine,” *IEEE Transactions on Magnetics*, Vol. 47, No. 10, 4238–4241, Oct. 2011.
16. El-Refaie, A. M., “Fractional-slot concentrated-windings synchronous permanent magnet machines: Opportunities and challenges,” *IEEE Transactions on Industrial Electronics*, Vol. 57, No. 1, 107–121, Jan. 2010.
17. Li, W. and K.-T. Chau, “Analytical field calculation for linear tubular magnetic gears using equivalent anisotropic magnetic permeability,” *Progress In Electromagnetics Research*, Vol. 127, 155–171, 2012.
18. Wang, Y., K. T. Chau, C. C. Chan, and J. Z. Jiang, “Transient analysis of a new outer-rotor permanent-magnet brushless dc drive using circuit-field-torque time-stepping finite element method,” *IEEE Transactions on Magnetics*, Vol. 38, No. 2, 1297–1300, Mar. 2002.